Design and Implementation of a LLC Resonant Solid State Transformer

Mohammad Rashidi[1], Necmi Altin[2,3], Saban Ozdemir[2,4], Abedalsalam Bani-Ahmed[1], Mohamad Sabbah[1], Farhad Balali[2], and Adel Nasiri[2]
[1] EATON Research Labs – Eaton, W126N7250 Flint Drive | Menomonee Falls, WI 53051
[2]Center for Sustainable Electrical Energy Systems, University of Wisconsin-Milwaukee, Milwaukee, WI, USA
[3] Department of Electrical & Electronic Engineering, Faculty of Technology, Gazi University, Ankara, Turkey
[4]Department of Energy Systems Engineering, Faculty of Technology, Gazi University, Ankara, Turkey
morashidi@eaton.com, altin@uwm.edu, ozdemir@uwm.edu, SalamABaniahmed@eaton.com, msabbah@uwm.edu, nasiri@uwm.edu

Abstract — In this study, analysis and control of a highly efficient, high power full-bridge unidirectional resonant LLC solid state transformer is discussed. A combination of Pulse Frequency Modulation (PFM) and Phase Shift Modulation (PSM) is utilized to control this resonant converter for a wide load range. The converter is designed to maintain soft switching by using a resonant circuit to minimize the switching loss of the high frequency converter. Zero-voltage-switching (ZVS) is achieved for the H-bridge converter. The ZVS boundary for the proposed combined control method is also analyzed in detail. The experimental setup for the suggested configuration was implemented, and the performance of the proposed control scheme and resonant LLC solid state transformer have been verified with test results. The proposed combined control scheme improves control performance. The obtained results show that, the proposed system can regulate output voltage and maintain soft switching in a wide range of load. Thus, the efficiency of the system is improved and an efficiency of 97.18% is achieved.

Keywords— DC/DC converter, resonant converter, soft-switching, solid state transformer.

I. INTRODUCTION

The Solid-State Transformer (SST) is a type of power electronics converters, which can properly meet the requirements of the new grid architecture [1]-[3]. The SST is a combination of a high- or medium-frequency transformer and multiple power electronics converters [4]. Medium - or high-frequency SSTs are becoming very common due to their superior advantages such as providing galvanic isolation, preventing common mode circulating current, extending step up/down range, and improving protection capabilities in a compact size [5], [6]. The size and weight reduction is the main motivation behind the studies on SSTs, since it directly affects the system initial investment and operational costs. In addition, their voltage and power level increase with the recent introduced soft magnetic materials and high frequency-high voltage semiconductor switches [7].

Furthermore, having multiple power electronics stages in a SST empowers online monitoring and active control of the system parameters. Integration of a SST into the grid can potentially offer several functionalities in a smart grid configuration including protecting each of the loads and power system from disturbances at the other side, providing DC ports for direct integrating of distributed generation and energy storage systems, and active supporting of the voltage and power profiles [8], [9]. However, the high switching loss in the multiple high-frequency conversion stages of the converter is one of the main challenges in realizing efficient SST topologies for different applications [10]-[12].

Although, full-bridge PWM converters are very common in the SST applications, increasing of the switching losses due to the high frequency switching, limits the level of the practical high frequency operation and size improvement of the SST [13], [14]. Therefore, the phase-shifted full bridge (PSFB) and dual-active bridge (DAB) converters, providing zero-voltage-switching (ZVS), are used in the SST applications. Even though these converters provide ZVS for primary switches, ZVS is lost at lower load conditions. Several techniques are introduced to extend the ZVS operation range. However, these techniques suffer from high circulating current [14], [15], and they usually require additional components which increase the system cost and complexity.

Achieving soft-switching through resonant circuit is an effective solution to tackle this problem. This can significantly improve the efficiency of the converter. Different resonant SST configurations have been discussed in the research papers. A LLC converter based SST is presented in [16] for constant voltage applications. Since both input and output voltages are considered as constant in this article, the switching frequency is kept constant at 20kHz and 93% efficiency is obtained [16]. A topology for a CLLC resonant SST is presented in [17]. This topology provides soft switching for a bidirectional low voltage DC-DC converter which is beneficial for applications like uninterruptible power supply and 97.8% maximum efficiency value is obtained. In this paper, a complex dead-band control at sub-resonant frequency is used, and the switching frequency is limited at the resonant frequency. The LLC resonant converters are illustrated in multiple studies [15], [18]–[19]. In general, the LLC resonant converter topologies enable ZVS and high power factor for the resonant tank [18]. The focus of the research in [18] is on reducing the leakage inductance to

improve the efficiency. To achieve this goal a resonant capacitor is connected in parallel to the magnetizing inductor through an auxiliary winding. It is reported that 92.5% efficiency is obtained with 300W prototype. In [15], a hybrid topology including an LLC resonant converter and a DAB converter is introduced and analyzed to combine the advantages of both topologies. While the LLC resonant converter operates at its resonant frequency and supplies the load for low load conditions, the DAB and LLC resonant converters supply load together for higher load conditions to extend the ZVS operation range. However, the efficiency values are not presented. This paper mainly focuses on the mathematical modeling of the configuration and control scheme for the voltage and current adjustment.

The aforementioned LLC converter solutions mostly employ pulse frequency modulation (PFM) method to control the output voltage. This method is developed based on the gain equation of the LLC converter. However, in the case of higher input or lower output voltages than designed values or low load conditions, very high switching frequencies are required. In addition, higher magnetization inductance values, which is chosen to limit the circulation current and improve the efficiency, decreases the slope of the gain curve. This results in a higher switching frequency requirement for the same gain. This high frequency value may limit the practical applications or decrease the efficiency of the converter.

The Phase-Shift Modulation (PSM) method is another control scheme applied to control the LLC resonant converters. In this method, a phase-shift is applied between the full-bridge inverter legs, and thus a second gain coefficient, which is independent from the switching frequency, is obtained. This second gain can be controlled between 0-1 with the phase-shift angle. This enables limiting the maximum switching frequency and provides a wider range to select optimal magnetization inductance to reduce circuiting current, and improves the efficiency. In [20] and [21], the PSM control is only applied during the startup process to limit the inrush current. The switching frequency is kept at its maximum value, and then phase-shift is linearly increased until half of the period to obtain smooth startup performance. However, the efficiency improvement via the PSM is limited at startup. In some applications, especially in constant power applications when very narrow regulation is required, the LLC resonant converter is designed to operate in the vicinity of the resonance frequency that they are theoretically the most efficient, and switching frequency is kept constant at this value. The gain is controlled with PSM method [22]. Some topologies which employ auxiliary active and passive components with modified phase-shift control method, are also presented to obtain wide operation range at constant switching frequency by sacrificing the simplicity of both converter topology and controller [23], [24]. In [25], the maximum switching frequency is defined as the resonant frequency, and when it is reached, the switching frequency is kept constant and the PSM is used to control. This method enables more optimal LLC resonant tank design. However, the main efficiency improvement is obtained for low load conditions. In this topology, for the heavy load conditions, the operation frequency is not close to the resonant frequency that gives the maximum efficiency. In [26], the PSM is applied to LLC resonant converter to limit the switching frequency for the low load conditions. The PFM is used to control the output voltage of the converter. Once the defined maximum frequency is reached, the switching frequency is kept constant at its maximum value, and the PSM is applied to control the converter. This combinational method is helpful to improve the efficiency at only low load conditions by limiting the required switching frequency. In [27], while only the PSM is applied for the heavy load conditions, the PSM and PFM are together applied for low load conditions. Then, instead of closed loop control, a linear equation which is optimized according to the loss calculation is employed, and active duty cycle width is calculated depending on load current. The switching frequency is also a linear function of the active duty cycle value. Again, the combined method is only helpful for the low load conditions.

In this paper, an LLC series resonant SST topology which enables achieving a relatively higher efficiency is developed, designed, implemented and tested. The topology of the proposed SST is depicted in Fig. 1. A combination of PFM and PSM methods is used to regulate the voltage and to cover a wide range of power levels with relatively lower switching frequency. Different from the past studies, the switching frequency and phase-shift are controlled together to regulate the voltage for all operation area. This enables the optimal transformer design to reduce the circulating current and conduction losses. Thus, relatively reduced average switching frequency is obtained, the power losses due to high frequency is reduced, and an efficient and compact SST design is achieved.

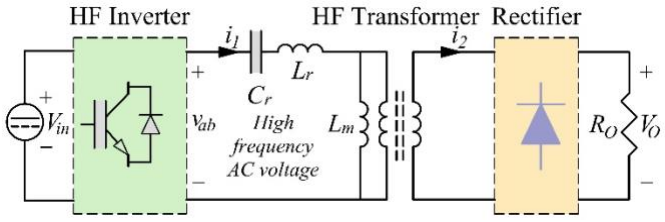

Figure 1. Resonant Solid State Transformer configuration.

II. CIRCUIT ANALYSIS FOR THE RESONANT SST

The LLC resonant tank acts as a band-pass filter for the square wave voltage at the terminals of the full-bridge converter. This results in a pseudo sinusoidal current at the primary side of the transformer. The detailed circuit representation of the proposed topology is presented in Fig. 2. In the general modes of operation, the controlled switch network produces a square wave output voltage, v_{ab}. The frequency of this voltage is close to the resonant frequency of the tank. Then, the output voltage of the resonant tank is

rectified to produce the DC load voltage, v_o. The input impedance of the system can be modified by changing the switching frequency, f_s to change the DC output voltage. In this case, the resonant tank responds primarily to the fundamental component of the voltage waveform and has negligible response at the harmonic frequencies $(2n+1)f_s$, n=1,3,5,7… [28], [29]. The Fundamental Harmonic Approximation (FHA) is used to obtain a transfer function that describes the gain of the resonant tank. The resulting equivalent circuit for FHA analysis is also given in Fig. 2.

A. Circuit Analysis:

The proposed resonant converter in this study operates using PFM and PSM methods. It is operated by turning off one set of the H-bridge leg earlier than the other set. The imposed phase-shift between the two legs creates three different levels on the output of the inverter: $+V_{in}$, $-V_{in}$, and 0. Thus, there is a discontinuity in the current every half period, which results in DCM operation at super-resonant frequency.

The design aims to ensure ZVS operation of the converter at different load conditions. The converter operates under varying switching frequency and phase-shift between the legs of the H-bridge. As a result of this operation, ZVS operation occurs at primary side switches during the turn-on and ZCS operation occurs at rectifier diodes during the turn-off.

The input voltage of the resonant tank $(v_{ab}(t))$ is a square wave varying between $-V_{in}$ and $+V_{in}$. Using Fourier series, the input voltage can be expressed by (1) [17].

$$v_{ab}(t) = \frac{4V_d}{\pi} \sum_{n=1,3,5,\dots}^{\infty} \frac{1}{n} sin(2\pi n f_s t) \quad (1)$$

The fundamental component of $v_{ab}(t)$ can be obtained by using n=1 as in (2):

$$v_{ab,1}(t) = \frac{4V_d}{\pi} sin(2\pi f_s t) \quad (2)$$

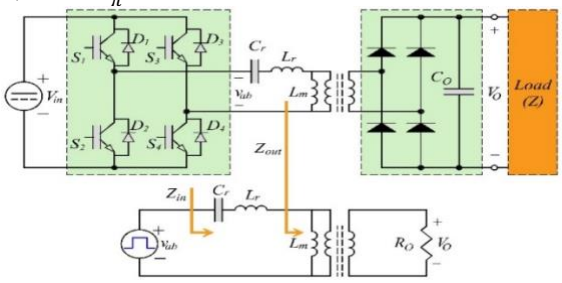

Figure 2. Detailed circuit of proposed SST & LLC resonant converter using the FHA analysis.

Equation (2) does not consider a varying phase-shift between the two legs of the inverter. If this phase-shift is represented by angle 'α', the output voltage of the inverter can be written as:

$$v_{ab\_\alpha n}(t) = \frac{4}{\pi n} V_d \, cos\left(\frac{1}{2}\alpha\right) sin(2\pi n f_s t) \quad (3)$$

The effective output load resistance seen in parallel with the magnetizing inductance L_m is defined as R_e. This accounts for the transformer turn ratio (N) and the output load (R_o). By using FHA, R_e can be written as follows:

$$R_e = \frac{8}{\pi^2} N^2 R_0 \quad (4)$$

The transfer function of the resonant circuit, defined as the ratio of the output voltage over the input voltage is shown in (5).

$$H_r = \frac{V_{0,FHA}}{V_{ab,FHA}} = \frac{\frac{sL_m * R_e}{sL_m + R_e}}{(sC_r)^{-1} + sL_r + \frac{sL_m * R_e}{sL_m + R_e}} \quad (5)$$

The normalized frequency, f_n can be written as a function of the switching frequency, fs and the first resonant frequency, f_{r1} as follows:

$$f_n = \frac{f_s}{f_{r1}} \quad (6)$$

where

$$f_{r1} = \frac{1}{2\pi\sqrt{L_r C_r}} \quad (7)$$

The quality factor, Q and the resonant tank impedance, Z_r and the inductance ratio, k are given by:

$$Q = \frac{Z_r}{R_e}; \quad Z_r = \sqrt{\frac{L_r}{C_r}}; \quad k = \frac{L_r}{L_m} \quad (8)$$

Using the above terms, H_r can be reformulated as follows:

$$H_r = \frac{\frac{jf_n}{k}}{\left[\frac{Q}{k} - \frac{f_n^2 Q}{k}\right] + j\left|f_n + \frac{f_n}{k} - \frac{1}{f_n}\right|} \quad (9)$$

The magnitude of H_r is obtained and evaluated at $(j2\pi f_s)$ as follows:

$$|H_r| = \left| \frac{\frac{jf_n}{k}}{\left[\frac{Q}{k} - \frac{f_n^2 Q}{k}\right] + j\left[f_n + \frac{f_n}{k} - \frac{1}{f_n}\right]} \right| \quad (10)$$

B. Gain Curve Analysis:

The gain curve of the resonant converter can be plotted using following equation as in Fig. 3:

$$|H_r| = \frac{\frac{f_n}{k}}{\sqrt{\left[\frac{Q}{K} - \frac{f_n^2 Q}{k}\right]^2 + \left[f_n + \frac{f_n}{k} - \frac{1}{f_n}\right]^2}} \quad (11)$$

There are two resonant frequencies, f_{r1} and f_{r2}, in Fig. 3. The second resonant frequency (f_{r2}) can be calculated by adding transformer magnetizing inductance to the resonant inductance as in (12).

$$f_{r2} = \frac{1}{2\pi\sqrt{(L_r + L_m)C_r}} \quad (12)$$

The gain of the resonant converter has to be monotonically decreasing when the operating frequency increases. Taking the derivative of (11) and setting it to less than zero, the following inequality is obtained:

$$Q < \sqrt{\frac{B(f_n)}{A(f_n)}} \quad (13)$$

where $A(f_n)$ and $B(f_n)$ are given as follows:

$$A(f_n) = f_n^4\left(\frac{-1}{2k^2}\right) + f_n^2\left(\frac{-1}{k}\right) + \frac{1}{k^2} \quad (14)$$

$$B(f_n) = f_n^2\left(\frac{1}{k^2} + \frac{2}{k} - \frac{3k}{2} + \frac{1}{2}\right) + \left(\frac{-2-2k}{k}\right) + \frac{3}{2f_n^2} \quad (15)$$

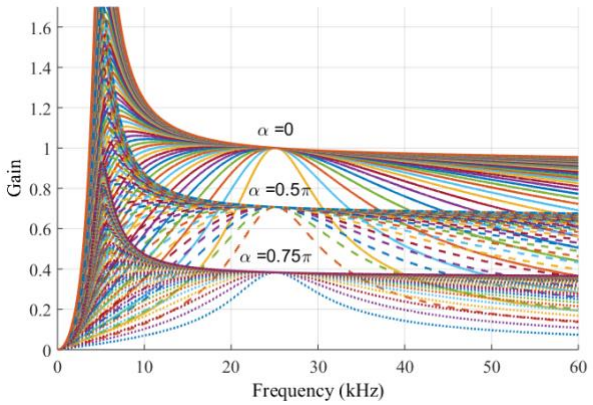

Figure 3. Resonant converter gain plot versus normalized frequency at various values of Q for different Alpha values.

The load resistance, R_o can be expressed as a function of the output voltage and output current. Using the condition obtained in (13), a condition for the maximum load current, $I_{o,max}$, can be derived as follows:

$$I_{o,max} < \frac{8V_oQ_{max}}{\pi^2 Z_r} \tag{16}$$

Alternatively, a condition for maximum Z_r at a given $I_{o,max}$ can be derived:

$$Z_r < \frac{8V_oQ_{max}}{\pi^2 I_{o,max}} \tag{17}$$

C. Soft-Switching Analysis

For all of the switches, ZVS at turn on is very important to minimize loss and stress. There are two key conditions for the conventional PFM controlled LLC resonant converters. It is well known that ZVS can be achieved only if the resonant current is lagging resonant tank voltage. So, the input impedance of the resonant circuit has to be inductive. The phase angle of the input inductance is given in (18):

$$\theta = tan^{-1}\left[-\frac{f_n^4Q^2+f_n^2k^2+f_n^2k-f_n^2Q^2-k^2}{f_n^3Q}\right] \tag{18}$$

Then, the first condition for ZVS can be written as $\theta \geq 0$.

Althhough the lagging resonant current is mandatory to obtain ZVS, it does not guarantee ZVS by itself. The output capacitors of the switches (which are going to turn on) and the parasitic capacitances have to be discharged in order to turn on the body diode within the dead time. In addition, the output capacitors of the switches which are turning off, have to be charged at the same interval. Since during the dead time the resonant current equals the magnetization current, the magnetizatin current should charge and discharge these capacitors within the dead time. The magnetization current value is related to the V_{in} and L_m. Since the required voltage gain and circulatig current values are affected by L_m, the dead time should be determined carefully by considering L_m, f_{sw}, and total capacitance of these switch output capacitors and parasitic capacitances (C_s). The minimum dead-time duration required to ensure ZVS is described as:

$$t_d \geq \frac{V_{in}C_s}{i_r} = 4C_sf_sL_m\,. \tag{19}$$

However, in case of the PSM, the first ZVS condition becomes more complex. When the PFM is applied, the angle of the input inductance is dependent to the switching frequency and parameters of the resonant tank component. Therefore, according to the tank parameters, the boundary of the lagging current and ZVS operation can be determined, and the lowest value of the switching frequency can be limited to ensure ZVS operation. However, when the PSM is employed the fundamental component of the input voltage equation can be written as given below:

$$v_{ab,1}(t) = \frac{4V_d}{\pi} sin\left(\frac{\pi-\alpha}{2}\right) sin(2\pi f_s t) \tag{20}$$

The inverter output voltage and resonant current waveforms for PSM control are given in Fig. 4 (a). As it is seen from figure, the phase-shift angle (α) generates a zero volt intervals on the output voltage waveform. Although, the input impedance angle is not affected by PSM control, because of the zero-volt intervals, the angle between zero-crossings of the resonant current and the voltage of the resonant tank varies. In some conditions, zero-crossing of the resonant current can lead the zero-crossings of the resonant tank voltage [30]. This results in losing ZVS operation. Therefore, the ZVS condition for PSM should be modified. The constraint should focus on the angle (φ) between zero-crossings of the resonant tank voltage and the resonant current. The zero-crossing of the resonant tank voltage should lead the zero-crossing of the resonant current to ensure achieving ZVS. This condition can be defined as in (21).

$$\varphi = \theta - \frac{\alpha}{2} \geq 0 \tag{21}$$

As it is seen from Fig. 4(a), the resonant tank voltage zero crossings are leading the resonant current zero crossings, and thus ZVS is achieved. However, increasing phase-shift angle value decreases the phase angle (φ) between the resonant tank voltage and current. For one phase-shift value, φ becomes zero as shown in Fig. 4(b). At this moment, the system is operating at the boundary of ZVS condition. Any further increase in phase-shift makes φ negative as depicted in Fig. 4(c). In this condition, the resonant current is leading the resonant network voltage, the ZVS operation is lost. For simplicity, the current waveform is assumed to be in sinusoidal waveform and constant for different phase-shift angle values in Fig. 4.

As it is discussed above, the phase-shift angle has an effect on ZVS, and higher values of the phase-shift angle may cause losing ZVS even when the impedance angle is positive. As explained in (21), the ZVS operation depends on the phase-shift and impedance angle values. As given in (18), the impedance angle depends on the switching frequency and the load. Therefore, controlling the frequency with the phase-shift angle can provide wider ZVS range for different load conditions. Therefore, the proposed system is analyzed for different load and switching frequency values, and variation of the impedance angle is investigated, considering (21) to provide better understanding about ZVS boundaries. The

variation of φ versus f_s and duty cycle (D) is given in Fig. 5. The color bar at the right side of the figure shows φ in degree. Except the red colored area, it is positive, and ZVS is achieved ($\varphi \geq 0$). As it is seen, for low load conditions the proposed system has a quiet wide ZVS range. For R_o=20Ω, the proposed system in ZVS region even with 30kHz. However, the ZVS range is narrowed for the heavier load conditions. It is seen that for R_o=3.5Ω, the converter can operate with ZVS for D≥0.32 at 30kHz switching frequency. If the switching frequency is increased to 60kHz, the ZVS region is extended to D≥0.2. This situation is valid for the lower duty cycle values. For the lower duty cycle values, higher switching frequency value is required to achieve ZVS. On the other hand, the higher duty cycle value is mostly required for low load conditions. It is clear that except the soft-start, the proposed converter operates in ZVS region for any value of the load.

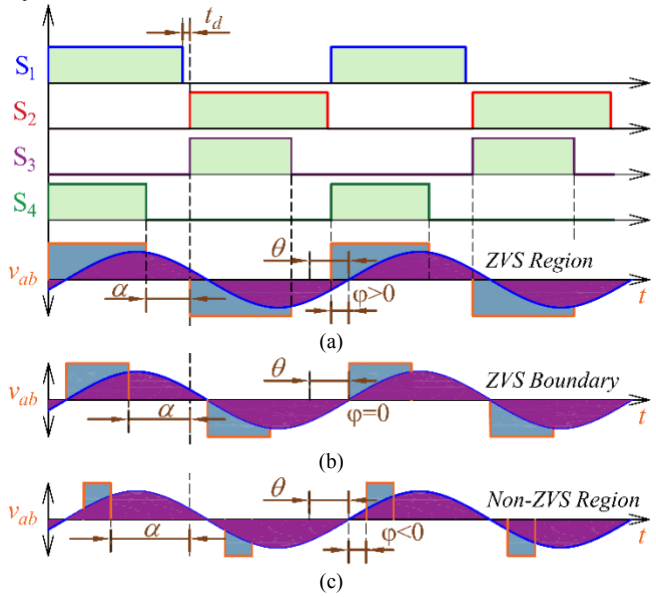

Figure **4**. The switching signals, generated resonant tank voltage (v_{ab}) and current (i_r) (a) when the system is operating in the ZVS region, b) The generated resonant tank voltage (v_{ab}) and current (i_r) when the system operating at the ZVS boundary, c) The generated resonant tank voltage, (v_{ab}) and current (i_r) when the system operating outside of the ZVS region.

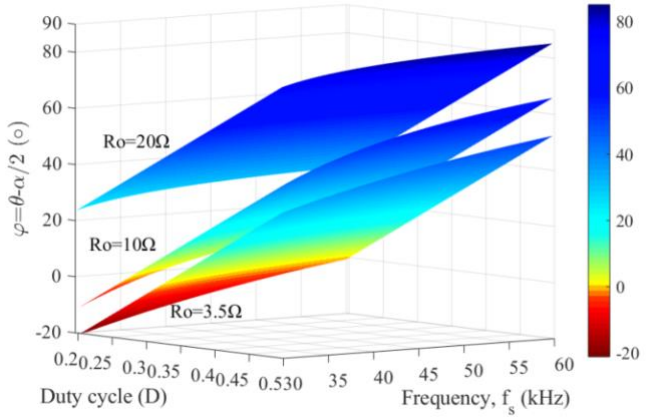

Figure 5. ZVS boundaries for different switching frequency, duty cycle and load values.

III. Controls

It is extremely important to maintain a regulated output DC voltage to support the varying load requirement. Generally, the PFM method is applied to the LLC resonant converter applications. According to (11), if the resonant tank parameters and the load are considered to be constant, the gain of the converter is related to the ratio of the switching frequency (f_s) and the resonant frequency (f_{r1}). It is clear from Fig. 3 that if the switching frequency is above the second resonant frequency (f_s>f_{r2}), increase in the switching frequency (f_s) results a decrease in the converter gain. In other words, the PFM method uses the variable switching frequency to adjust the operation point on the gain curve. The converter gain is equal to "1" at f_s=f_{r1}. If f_s>f_{r1}, the gain is <1. The gain decreases with the increasing frequency. This feature can be used especially at low load conditions. However, k has significant impact on this gain reduction rate of the increasing switching frequency. Although higher k value increases the effect of switching frequency on gain (reduces the required maximum switching frequency value) it causes higher circulating current which results in higher power loss, and reduces efficiency. The circulating current can be reduced by selecting smaller k value with the expense of higher switching frequency requirement to reach the minimum voltage gain. Therefore, design of the LLC resonant converter is a complex subject. In addition, control of the LLC converter providing fast transient response and safe start-up is another challenge especially for the wide-range of variable load or variable output voltage applications. These requirements could negatively affect the optimal efficient design of the converter. Hence, in this study, the PFM and PSM methods are combined and used to control the output voltage of the LLC resonant SST.

It can be seen from (5) that output voltage also depends on the input voltage. The PSM method is used to control the input voltage in (5) and provide another control variable to regulate the output voltage. In the PSM method, a phase-shift angle is introduced between the full bridge inverter legs. If the gate signals of the S_3 and S_4 are shifted with a phase-shift angle "α", some overlaps appear and generate zero voltage states at the inverter output voltage. In this study, instead of shifting the phase of the gate signals of the S_3 and S_4, the duty ratio of these gate signals are controlled, which ultimately has the same result as shifting between two pairs of a four-switch H-Bridge configuration. By adjusting the duty ratio of S_3 and S_4, zero voltage state seen at the terminals of the inverter is increased or decreased. The gate signals of the switches and resultant inverter voltage is shown in Fig. 4(a). In this case, output voltage equation changes to (3) and phase-shift angle "α" (or duty cycle, D ($D = (\pi - \alpha)/2\pi$) is introduced as a new control variable. Although, the output voltage can be controlled from zero to its maximum value with the phase-shift angle in an H-Bridge configuration, higher values of this angle leads to losing ZVS, and hard switching. Therefore, a

combination of these two control schemes, PSM and PFM, is utilized to control the converter.

By using both PFM and PSM methods, it is possible to support a wider range of load. Adjusting phase-shift angle enables holding a specific switching frequency for a varying load. Alternately, the converter can be operated at the lower switching frequencies with higher phase-shift angle values for a fixed load. Fig. 6 shows graphs of f_s versus duty ratio (D) obtained from calculation and simulation studies for two different load requirements that are fixed at 35A and 70A. Here the duty ratio is the length of the inverter output voltage which is equal to $(\pi - \alpha)/2\pi$). In this case, decreasing both f_s and duty cycle allows the controller to support a fixed load requirement and regulate a specific desired voltage level. Fig. 7 shows that a wider range of output voltage is realized when both PFM and PSM methods are used together. Whereas conventional PFM controlled converter has a fixed gain curve (for a fixed load), the proposed one has multiple curves for each duty cycle value. The converter would operate at any point depending on f_s and duty ratio.

The proposed control scheme employs PFM and PSM methods and controls all of the variables at the same time properly. As it was mentioned before, this control scheme can be designed to keep the switching frequency constant or keep the switching frequency as low as possible for the whole operation range to decrease the switching losses. However, lower duty cycle value causes distorted resonant currents which also causes additional power losses. In addition, operation below the boundary of duty cycle value also causes losing ZVS and increases the losses. In this study, a combined control scheme is designed and used to obtain higher efficiency which keeps the switching frequency between the defined upper and lower limits, and keeps duty cycle value over a ZVS boundary value except the soft-start and very abrupt conditions.

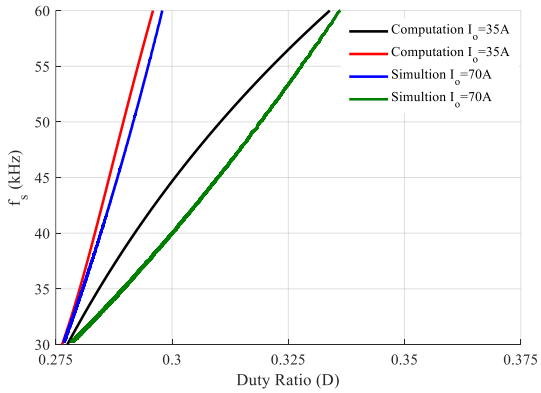

Figure 6. Switching frequency versus duty ratio

The block diagram of the proposed control system is shown in Fig. 8. The controller is a classical cascaded loop, where the outer loop which receives voltage feedback and generates a reference signal for current loop. Since the current has faster dynamic in compare to the voltage, the two-loop controller is preferred to improve the transient response which ultimately adjust the resonant current for voltage regulation [31]. The reference signal of the resonant current is generated by voltage PI controller using output voltage error. Instead of the load current, the resonant current is used in the current control loop. The current error is calculated with this reference current and actual current obtained by filtering the actual resonant current. A first order low pass filter given in (22) is used to filter the resonant current.

$$\boldsymbol{F(s)} = \frac{\mathbf{1}}{\mathbf{1}+\frac{\boldsymbol{s}}{\mathbf{2\pi f_1}}} \tag{22}$$

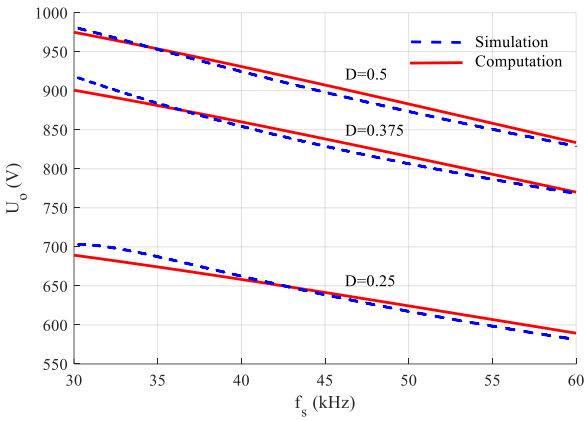

Figure 7. V_o at different duty ratios (D) for a spectrum of f_s.

The switching frequency is determined according to the required phase-shift value. The minimum switching frequency value f_{s_min} is determined according to the resonant frequency f_{r1} to ensure the ZVS. Proper selection of the K_f gain, also limits the maximum switching frequency. The switching frequency and duty cycle calculation and switching pulse generation are implemented with a state machine block.

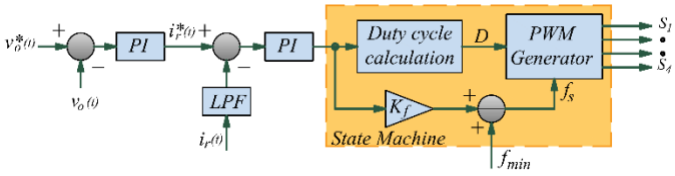

Figure 8. Proposed control scheme employing combination of the PFM and the PSM methods.

Table 1: Parameters of the system

Parameters	**Value**
Resonant inductor, L_r	10µH
Magnetizing inductor, L_m	250µH
Resonant capacitor, C_r	4µF
Filter capacitor, C_0	450µF
Voltage controller	K_p=1.5, K_i=2000
Current Controller	K_p=0.2, K_i=1800
Input voltage, V_{in}	700V

IV. Simulation and Experimental Results

The performance of the proposed LLC resonant converter based SST is tested by simulations and experimental tests. The experiments are performed on a 150kW prototype. Simulations are done in MATLAB/Simulink. In the experimental study, full bridge inverter, high current resonant capacitor, high frequency transformer, full bridge rectifier and filter capacitors are used. The leakage inductance of the transformer is used as the resonant inductor. The system parameters are given in Table I. The proposed control system is implemented with a FPGA. The switching frequency range is defined as 30-60kHz.

The experimental results for the output DC voltage (v_o) of the full bridge inverter, the output AC voltage of the full bridge inverter (v_{ab}) and resonant current (i_r) are shown in Fig. 9. This figure shows that the output voltage is tracking its reference voltage successfully. There is not any oscillations or overshot with the proposed control system combines PFM and PSM methods. The experimental results for start-up and steady state operation is also seen in figure. As it can be easily seen, there is a great harmony between the simulation and experimental results.

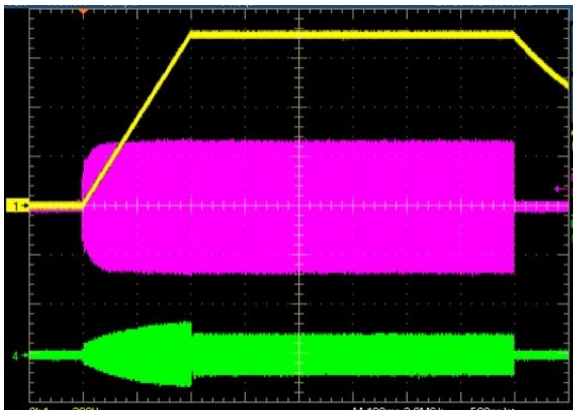

Figure 9. The output DC voltage of the full bridge inverter (Ch.1, yellow), the output AC voltage of the full bridge inverter (Ch.3, pink) and resonant current (Ch.4, green) showing start-up to steady state duration.

In Figs. 12 and 13, the simulation and experimental results for the start-up duration is depicted. Start-up is a challenge for the conventional PFM controlled LLC resonant converters due to the maximum switching frequency limit. The proposed control algorithm controls both frequency and duty cycle of the switching signals applied to the full-bridge inverter. Thus, more sufficient control on the voltage gain and the output DC voltage of the converter is obtained. When the inverter output voltage is checked, it is seen that the pulse width of the inverter voltage is very small at the beginning and it is increasing to remove the error between the reference and actual voltages. Obviously, there is a direct relation between the inverter voltage and the resonant current, and the resonant current is also increasing with the increasing inverter voltage. The proposed system is also tested for the light load conditions. Experimental results for 15kW load power condition are given in Fig. 12. It is seen that, the simulation and experimental results are similar to each other. Since the load power is low, the controller keeps the duty cycle low, and therefore, the inverter voltage has long zero states. Therefore, the resonant current is distorted.

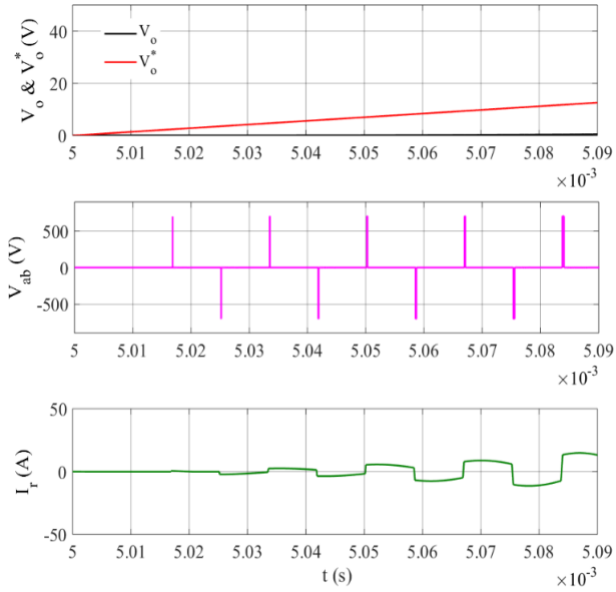

Figure 10. Simulation results for start-up.

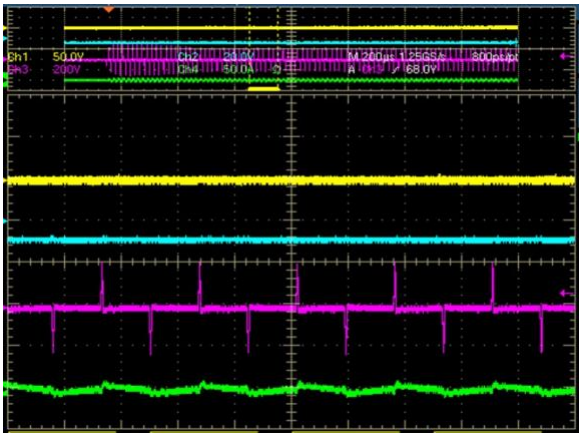

Figure 11. Experimental results for the output DC voltage (Ch.1, yellow), the inverter voltage (Ch.3, pink) and resonant current (Ch.4, green) during showing the start-up.

In Fig. 13, experimental results are given for the high load conditions. The proposed SST is tested with 140kW load, and output DC voltage, the inverter voltage and the resonant current are depicted. The proposed controller has decreased the duty cycle and thus shortened the zero states on inverter voltage waveform. Now, the resonant current is close to sinewave. The output voltage is stable at its desired value and steady state error is removed. The proposed LLC resonant converter based SST achieves ZVS for the full-bridge inverter for wide operation range. The efficiency of the proposed system is also investigated and the maximum efficiency of the system is measured as of 97.18%.

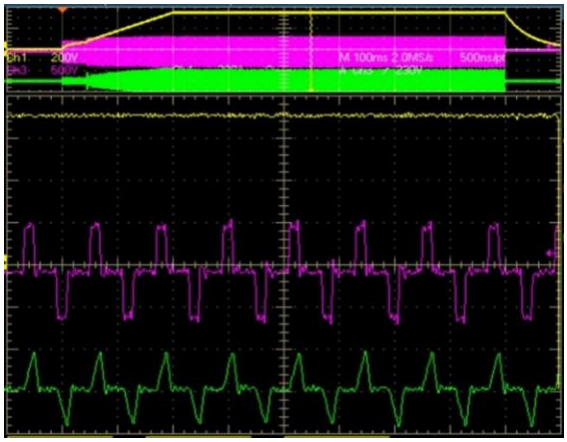

Figure 12. Experimental results for light load (15kW) operation conditions (the output DC voltage (Ch.1, yellow), the inverter voltage (Ch.3, pink) and resonant current (Ch.4, green)).

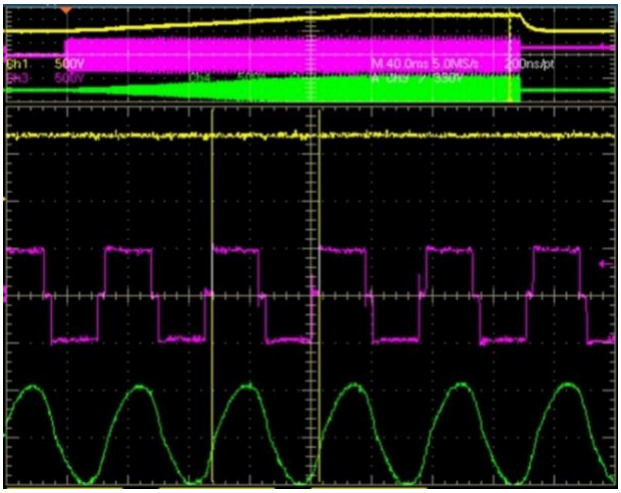

Figure 13. Experimental results for high power (140kW) load condition (the output DC voltage (Ch.1, yellow), the inverter voltage (Ch.3, pink) and resonant current (Ch.4, green)).

V. CONCLUSIONS

In this study, a new control structure has been presented and tested for an LLC resonant converter based SST. The discussed topology has several advantages compared to the conventional topologies that rely only on transformers or power electronics circuitries. It provides load regulation, power flow control, and galvanic isolation. Soft-switching has been achieved by adding a properly designed resonant tank. A mathematical analysis was conducted and used to plot the gain curve of the converter. The ZVS constraint for PSM is also investigated. The proposed controller combines the PFM and PSM methods and adjusts the output voltage of the SST by varying the switching frequency and/or duty cycle values. The proposed cascaded controller defines the switching frequency and duty cycle values for any operation condition. The PSM method removes the higher switching frequency requirement. It also provides flexibility to determine the magnetization inductance and limits the circulating current. Thus the efficiency of the system is improved and 97.18% maximum efficiency is achieved. The achievable power level of the design is also extended. The experimental tests show similar results as the simulation, and prove the high dynamic and steady state performance of the proposed SST.

ACKNOWLEDGMENT

This material is based upon work supported by the National Science Foundation under Grant No. 1650470. Any opinions, findings, and conclusions or recommendations expressed in this material are those of the author(s) and do not necessarily reflect the views of the National Science Foundation. Dr. Necmi Altin and Dr. Saban Ozdemir also thank the financial support from the Scientific and Technological Research Council of Turkey (TUBITAK) BIDEB-2219 Postdoctoral Research program.

REFERENCES

[1] S. Falcones, R. Ayyanar and X. Mao, "A DC–DC multiport-converter-based solid-state transformer integrating distributed generation and storage," IEEE Transactions on Power Electronics, vol. 28, no. 5, pp. 2192-2203, May 2013.

[2] S. Hambridge, A. Q. Huang and R. Yu, "Solid State Transformer (SST) as an energy router: Economic dispatch based energy routing strategy," 2015 IEEE Energy Conversion Congress and Exposition (ECCE), Montreal, QC, 2015, pp. 2355-2360.

[3] M. Rashidi, A. Nasiri and R. Cuzner, "Application of multi-port solid state transformers for microgrid-based distribution systems," 2016 IEEE International Conference on Renewable Energy Research and Applications (ICRERA), Birmingham, 2016, pp. 605-610.

[4] M. Rashidi, M. Sabbah, A. Bani-Ahmed, A. Nasiri and M. H. Balali, "Design and implementation of a series resonant solid state transformer," 2017 IEEE Energy Conversion Congress and Exposition (ECCE), Cincinnati, OH, 2017, pp. 1282-1287.

[5] C. W. T. McLyman, Transformer and Inductor Design Handbook. CRC Press, 1964.

[6] Hengsi Qin and J. W. Kimball, "Ac-ac dual active bridge converter for solid state transformer,"2009 IEEE Energy Conversion Congress and Exposition, San Jose, CA, 2009, pp. 3039-3044.

[7] S. Ozdemir, S. Balci, N. Altin and I. Sefa, I., "Design and performance analysis of the three-level isolated DC-DC converter with the nanocyrstalline core transformer", International Journal of Hydrogen Energy, vol.42, no.28, pp.17801-17812, 2017.

[8] H. Zhao, T. Zhu, D. Cheng, B. Li, J. Ding and Y. Li, "Research on the smart modular cascaded solid state transformer interfaced to distributed photovoltaic power generation system," The Journal of Engineering, vol. 2017, no. 13, pp. 1872-1879, 2017.

[9] J. W. Kolar, G. Ortiz, "Solid state transformer concepts in traction and smart grid applications" 28th Applied Power Electronics Conference and Exposition (APEC 2013): 2012.

[10] S. Xu, A. Q. Huang, R. Burgos, "Review of solid-state transformer technologies and their application in power distribution systems," IEEE Journal of Emerging and Selected Topics in Power Electronics, vol. 1, no. 3, pp. 186-198, 2013.

[11] L. Zhang, Z. Zhao and J. Qin, "Efficiency optimization design of DC-DC solid state transformer based on modular multilevel converters," 2017 IEEE Energy Conversion Congress and Exposition (ECCE), Cincinnati, OH, 2017, pp. 3508-3513.

[12] H. Fan and H. Li, "High-frequency transformer isolated bidirectional DC–DC converter modules with high efficiency over wide load range for 20 kVA solid-state transformer," IEEE Transactions on Power Electronics, vol. 26, no. 12, pp. 3599-3608, Dec. 2011.

[13] K. Murata and F. Kurokawa, "An interleaved PFM LLC resonant converter with phase-shift compensation," IEEE Transactions on Power Electronics, vol. 31, no. 3, pp. 2264-2272, March 2016.

[14] Mohamad Sabbah, "Analysis, Design and Implementation of a Resonant Solid State Transformer," MSc. dissertation, Electrical Engineering Department, University of Wisconsin Milwaukee, Milwaukee WI, May 2016.

[15] C. Liu, H. Liu, G. Cai, S. Cui, H. Liu and H. Yao, "Novel hybrid LLC resonant and DAB linear DC–DC converter: Average model and experimental verification," IEEE Transactions on Industrial Electronics, vol. 64, no. 9, pp. 6970-6978, Sept. 2017.

[16] G. Ortiz, M. G. Leibl, J. E. Huber and J. W. Kolar, "Design and experimental testing of a resonant DC–DC converter for solid-state transformers," IEEE Transactions on Power Electronics, vol. 32, no. 10, pp. 7534-7542, Oct. 2017.

[17] Jung, J-.H.; Kim, H-.S.; Ryu, M-.H.; Baek, J-.W., "Design methodology of bidirectional CLLC resonant converter for high-frequency isolation of DC distribution systems", IEEE Transactions on Power Electronics, vol.28, no.4, pp.1741-1755, April 2013.

[18] R. L. Lin and L. H. Huang, "Efficiency improvement on LLC Resonant converter using integrated LCLC resonant transformer," IEEE Transactions on Industry Applications, vol. 54, no. 2, pp. 1756-1764, March-April 2018.

[19] K. Tan, R. Yu, S. Guo and A. Q. Huang, "Optimal design methodology of bidirectional LLC resonant DC/DC converter for solid state transformer application," IECON 2014 - 40th Annual Conference of the IEEE Industrial Electronics Society, Dallas, TX, 2014, pp. 1657-1664.

[20] D. Yang, C. Chen, S. Duan, J. Cai and L. Xiao, "A variable duty cycle soft startup strategy for LLC series resonant converter based on optimal current-limiting curve," IEEE Transactions on Power Electronics, vol. 31, no. 11, pp. 7996-8006, Nov. 2016.

[21] J. Jung, H. Kim, M. Ryu and J. Baek, "Design methodology of bidirectional CLLC resonant converter for high-frequency isolation of DC distribution systems," IEEE Transactions on Power Electronics, vol. 28, no. 4, pp. 1741-1755, April 2013.

[22] S. Chudjuarjeen, A. Sangswang and C. Koompai, "An improved LLC resonant inverter for induction-heating applications with asymmetrical control," IEEE Transactions on Industrial Electronics, vol. 58, no. 7, pp. 2915-2925, July 2011.

[23] H. Wu, T. Mu, X. Gao and Y. Xing, "A secondary-side phase-shift-controlled LLC resonant converter with reduced conduction loss at normal operation for hold-up time compensation application", IEEE Transactions on Power Electronics, vol.30 no.10, pp.5352-5357, 2015.

[24] E. S. Kim, J. Lee, Y. Heo and T. Marius, "LLC resonant converter with wide output voltage control ranges operating at a constant switching frequency", IEEE Applied Power Electronics Conference and Exposition, pp. 2124-2128, 2018.

[25] H. Pan, C. He, F. Ajmal, H. Chen and G. Chen, "Pulse-width modulation control strategy for high efficiency LLC resonant converter with light load applications," IET Power Electronics, vol. 7, no. 11, pp. 2887-2894, 11 2014.

[26] N. Shafiei, M. Ordonez, M. Craciun, C. Botting and M. Edington, "Burst mode elimination in high-power LLC resonant battery charger for electric vehicles," IEEE Transactions on Power Electronics, vol. 31, no. 2, pp. 1173-1188, Feb. 2016.

[27] J. Kim, C. Kim, J. Kim, J. Lee and G. Moon, "Analysis on load-adaptive phase-shift control for high efficiency full-bridge LLC resonant converter under light-load conditions," IEEE Transactions on Power Electronics, vol. 31, no. 7, pp. 4942-4955, July 2016.

[28] R. Erikson and D. Maksimovic, “Fundaments of Power Electronics”, Boulder CO: Springer Science and Business Media Inc., 1997, Ch. 19.

[29] N. Moohan: Resonant Converters, “Power Electronics: Converters, Applications and Design”. In Edited by Anonymous Minneapolis MN: John Wiley & Sons, 1989.

[30] N. Shafiei, M. Ordonez, M. Cracium, M. Edington and C. Botting, "High power LLC battery charger: Wide regulation using phase-shift for recovery mode," 2014 IEEE Energy Conversion Congress and Exposition (ECCE), pp. 2037-2042, Pittsburgh, PA, 2014.

[31] P. Krein, “Elements of Power Electronics” Oxford University Press, Pages:600-609, 1998.